Suppression of Eddy Current Loss in Multilayer NiFe-Polypyrrole Magnetic Cores Fabricated Using a Continuous Electrodeposition Process

Jun Beom Pyo, *Graduate Student Member, IEEE*, Xuan Wang, Minsoo Kim, *Member, IEEE*, Hanju Oh, *Member, IEEE*, Robert Kauffman, and Mark G. Allen, *Fellow, IEEE*

***Abstract*— Metallic magnetic alloys are of interest as core materials in ultracompact or integrated inductors and transformers. However, when operated at high frequencies, such materials should comprise a multilayer stack of magnetic material laminations and electrically insulating interlayers to suppress eddy current loss. To achieve scalable and continuous fabrication of such a structure, sequential multilayer electrodeposition is an attractive approach. To achieve sequential electrodeposition, interlayer's electrical conductivity should be sufficiently high to permit electrodeposition of subsequent layers, but sufficiently low to suppress eddy current loss. Polypyrrole, an electrodepositable polymer, was investigated as an interlayer material. Finite element modeling demonstrated a negligible difference in eddy current loss between NiFe/polypyrrole and NiFe/vacuum multilayers. Experimental verification of the efficacy was demonstrated as well. Compared with a single-layer NiFe inductor that has a comparable low-frequency (10 kHz) inductance value, a laminated ten-layer NiFe core showed higher inductance retention (88% of the low-frequency inductance for the laminated core versus 21% for the single-layer core) and lower ac resistance (1.68 versus 12.7 Ω) at 8 MHz, both of which are signs of suppressed eddy current. This scalable fabrication approach to high-frequency inductors will facilitate power converter miniaturizations.**

***Index Terms*— Eddy current suppression, high-frequency power converters, inductor, MEMS.**

I. Introduction

THE increasing complexity of electronic systems, including Internet of Things (IoT) devices, implantable bioelectronics, portable electronic devices, and electric vehicles, is driving interest in power converters for voltage shifting, power supply distribution, and battery interfacing. Furthermore, these systems often have volumetric or footprint constraints [1]–[4], which place concomitant restraints on the physical size of the power converters. Inductors are often the bottleneck in power electronic device size reduction, as magnetic components typically occupy large physical volumes within the converter [5]–[7]. To address this need, researchers have been working toward miniaturizing inductors while maintaining inductor performance [8]. Furthermore, as inductor sizes reduce, co-integration of magnetic components with drive electronics becomes possible, enabling the realization of power supplies on a chip (PwrSoC) [9]–[11], with the potential for reduced parasitics and cost improvements.

The choice of interlamination insulation material is dictated both by fabrication constraints and conductivity constraints. From a fabrication perspective, the material should be able to be electrodeposited so that it can easily be selectively placed in the magnetic core mold. From a conductivity perspective, the material should be chosen such that its conductivity is high enough to allow subsequent electrodeposition of magnetic and insulation layers in a stack, while at the same time is sufficiently low that eddy currents will be suppressed.

In general, the power-handling capacity of an inductor per unit core volume in a switching converter application is proportional to the product of the square of the core saturation flux density (B_s) and the frequency (f) of operation. Operation at high frequency, therefore, is often attractive when seeking to minimize the core volume. However, high-frequency operation can result in eddy current formation [12] in electrically conducting cores, typically restricting such cores to relatively lower saturation flux density ferrite materials.

If not for this eddy current generation, high saturation flux alloys of nickel, iron, and cobalt could be attractive materials as high-frequency inductor cores. One common strategy to suppress eddy current loss in such conducting cores is keeping the core thickness below the skin depth at the operation frequency of interest. However, the skin depth of typical metallic magnetic alloys in the low megahertz regime is typically on the order of several microns [7], [13], [14]. Since the power-handling capacity of the core is proportional to the core volume, such core thicknesses are typically unsuitable for conversion levels in the tens of watt range. The typical approach to address this issue is to stack multiple thin magnetic layer laminations, each bearing an electrically insulating interlayer,

Manuscript received 2 July 2021; revised 24 November 2021 and 1 March 2022; accepted 20 March 2022. Date of publication 25 April 2022; date of current version 6 December 2022. This work was supported in part by the NSF National Nanotechnology Coordinated Infrastructure Program of the Singh Center for Nanotechnology under Grant NNCI-2025608 and in part by EnaChip, Inc.. Recommended for publication by Associate Editor Maeve Duffy. *(Corresponding author: Jun Beom Pyo.)*

Jun Beom Pyo, Xuan Wang, and Mark G. Allen are with the Department of Electrical and Systems Engineering, University of Pennsylvania, Philadelphia, PA 19104 USA (e-mail: junpyo@seas.upenn.edu; wxuan@seas.upenn.edu; mallen@seas.upenn.edu).

Minsoo Kim and Hanju Oh were with the Department of Electrical and Systems Engineering, University of Pennsylvania, Philadelphia, PA 19104 USA. They are now with Apple Inc., Cupertino, CA 95014 USA (e-mail: novamagic@gmail.com; hanjuoh5@gmail.com).

Robert Kauffman is with the Department of Nanotechnology, University of Pennsylvania, Philadelphia, PA 19104 USA (e-mail: kauffrc@seas.upenn.edu).

Color versions of one or more figures in this article are available at https://doi.org/10.1109/JESTPE.2022.3166849.

Digital Object Identifier 10.1109/JESTPE.2022.3166849

to form the core. The insulating interlayers inhibit large eddy currents from forming by confining eddy currents to each magnetic lamination. Eddy current losses are then dictated by the individual lamination thickness, while the power-handling capability is dictated by the total core thickness. Such a lamination structure allows the simultaneous exploitation of high-frequency operation and high flux density material for inductor miniaturization.

A common method to fabricate a lamination structure for inductor cores is sequential sputtering [15]. However, sputtering is a relatively slow process, and deposition speeds and film stresses make it challenging to realize cores in many tens of microns thickness range using this approach. To construct thicker cores, electrodeposition has been widely adopted [6], [7], [13]. For example, a lamination structure can be achieved by sequentially electroplating magnetic material layers and metallic nonmagnetic interlayers after which the interlayers are selectively etched to create air gaps. Although this approach has been demonstrated [6], it typically requires a support structure to prevent layer collapse, increasing the complexity of fabrication. Another example is the liquid-assisted self-assembly of electroplated magnetic lamination layers, in which the liquid contains a dissolved polymer insulator. Individual magnetic layers are supported on an alignment guidewire, dipped into a liquid polymer solution, and pulled from the solution. Surface tension then self-assembles the magnetic sheets into a multi-layer lamination structure having an insulating polymer interlayer [16]. Although such an assembly method is useful in laboratory-scale research, it is challenging to use for integrated inductors in PwrSoC approaches. An improved approach would be a fully additive, continuous electrodeposition process in which laminations and interlayers are deposited without complex pre- or post-processing.

Such an approach places significant constraints on the interlayer material conductivity. Each material layer should be electrically conductive to achieve a continuous and additive electrodeposition process. However, the interlayers should be insulating to confine eddy currents to individual magnetic layers. Therefore, the interlayer material for the laminated inductor core should possess an intermediate conductivity. In [17], we have detailed the process of continuous additive electrodeposition and shown that conductive polymer polypyrrole (PPy) [18]–[20] is sufficiently conductive to enable subsequent sequential electrodeposition of metals. If at the same time the PPy interlayer is insulating enough so that it can suppress eddy current loss, it could be a promising interlayer material for a laminated inductor core.

In this article, we fabricate lamination magnetic core structures comprising nickel–iron (NiFe) as the magnetic material and PPy as the interlayer insulation, using a continuous and additive electrodeposition process. By characterizing the cores produced in this fashion, we analyze the effectiveness of PPy in suppressing eddy currents. NiFe was chosen as the magnetic material for its relatively high B_s. Finite element analysis was conducted to compare PPy interlayers with a hypothetical vacuum interlayer material over this frequency range. For empirical testing, three different inductor geometries (wire, solenoid, and toroid) were investigated. Each inductor geometry possessed a core comprising either a single thick layer of NiFe or two thin layers of NiFe with a PPy interlayer. In this latter case, each of the thin layers was half the thickness of the thick layer, so as to present the same total magnetic core volume. The inductance, ac resistance, and quality factor of each inductor as a function of frequency up to 8 MHz were determined. Finally, a core comprising ten layers of NiFe and nine PPy interlayers was fabricated to demonstrate the scalability of fabrication and the difference in electrical performance compared with an inductor with a single NiFe layer.

II. Validation of Eddy Current Suppression Through Finite Element Analysis

The choice of interlamination insulation material is dictated both by fabrication constraints and conductivity constraints. From a fabrication perspective, the material should be able to be electrodeposited so that it can easily be selectively placed in the magnetic core mold. From a conductivity perspective, the material should be chosen such that its conductivity is high enough to allow subsequent electrodeposition of magnetic and insulation layers in a stack, while at the same time is sufficiently low that eddy currents will be suppressed.

The question of suppression of eddy currents in lamination stacks has been previously examined analytically. Eddy current suppression depends on the conductivity ratio between the magnetic core material and the interlamination insulation [14], as well as the core fill factor and core width [14]. Based on these analytical models, and considering typical integrated inductor sizes, it was shown that a conductivity ratio of magnetic core to interlamination insulation above 10^6 is sufficient to suppress eddy current loss up to $\sim$10 MHz [14], [17] under the conditions that: 1) the thickness of an individual magnetic core lamination is below the typical skin depth of about a few micrometers; 2) the interlamination insulation layer thickness is in the sub-micrometer range; and 3) the cores are less than $\sim$1 cm in width. Another potential issue that might arise is loss due to the flow of displacement current through thin interlayers at high frequency, especially if the relative permittivity of the interlayer insulation layer is high. Even considering the high relative permittivity value of PPy of approximately 1000 [21], modeling demonstrates that cores with typical integrated inductor sizes mentioned above will generate displacement currents that have a negligible effect on eddy current loss up to $\sim$10 MHz [22].

To further validate the predictions of these models for eddy current suppression using PPy interlayer insulation, a 3-D finite element analysis using ANSYS Maxwell 3-D was conducted. The upper portion of Fig. 1(a) shows a perspective view of the modeled solenoid inductor structure. The lower portion of Fig. 1(a) shows in cross section the three different inductor core geometries that were simulated: a single-layer NiFe core, a two-layer NiFe core with vacuum as an interlayer, and a two-layer NiFe core with PPy as an interlayer. The total volume and total cross-sectional area of NiFe were the same for all the cases. The single-layer NiFe core was 17-mm long, 22-μm wide, and 2-μm thick. For the two-layer NiFe models, each NiFe lamination was 1-μm thick while PPy and vacuum

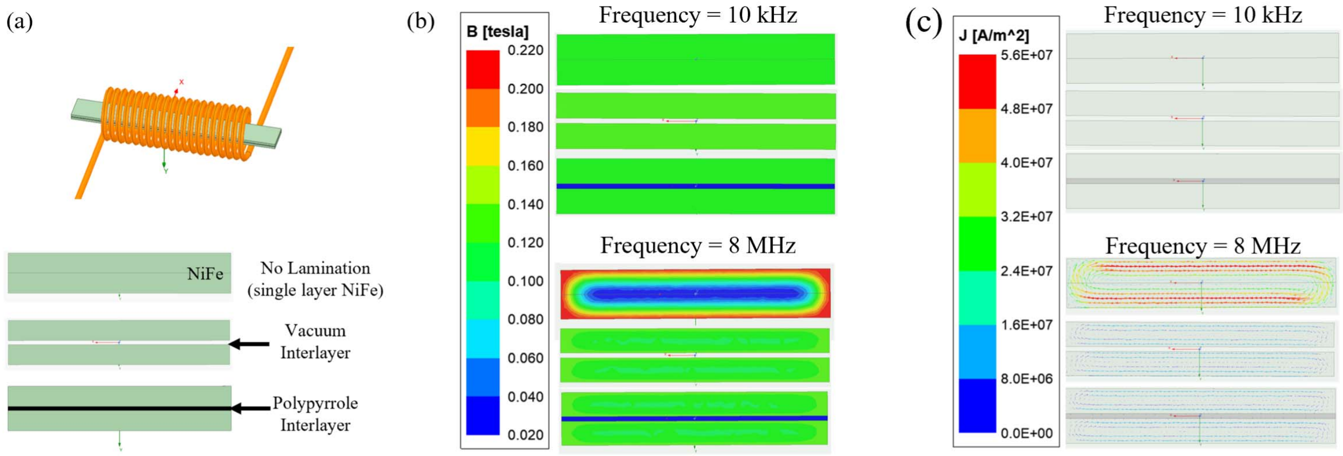

Fig. 1. (a) Three-dimensional solenoid model having magnetic core in the center and windings around the core used for finite element analysis (top) and cross sections of the three different types of cores analyzed (bottom). The green color represents NiFe, a white strip between NiFe layers represents a vacuum interlayer, and a black strip between NiFe layers represents a PPy interlayer. (b) Simulated magnitude of magnetic flux density plotted on these three different cross sections at 10 kHz and 8 MHz at a position midway along the length of the solenoid. (c) Simulated current density vector plotted on these three different cross sections at a position midway along the length of the solenoid at both 10 kHz and 8 MHz. The magnitude of current density is indicated by arrow color and size.

interlayers were 400-nm thick. Widths and lengths were the same as the single-layer NiFe core. The magnetic core was wound by a copper wire having 2.5-μm radius and 20 turns.

Simulations were conducted at operating frequencies of 10 kHz and 8 MHz to illustrate both the low-frequency and high-frequency behavior of the magnetic cores. The relative permeability of NiFe was taken as 800, and the conductivity was taken as 6.3×10^6 S/m. The relative permittivity and permeability of the vacuum interlayer were taken as unity, and the electrical conductivity of the vacuum interlayer was taken as zero. The relative permeability of the PPy interlayer was taken as unity, the relative permittivity as 1000, and electrical conductivity as 1.1 S/m. Note that the PPy conductivity was not set to the actual vertical conductivity value of 0.08 S/m [17] because the simulation program enables eddy current mode only when the material has conductivity higher than 1.1 S/m. Thus, this simulation will be a conservative estimate of the generated losses. During the simulation, both displacement current calculation and eddy current calculation were enabled.

If the high-frequency operation of these electrically conducting cores results in eddy currents, two phenomena should be observed. First, the eddy currents themselves should be noted within the core; and second, the core should have significant flux exclusion in portions of its cross-sectional area due to the canceling flux produced by the eddy currents. Therefore, an examination of both magnetic flux density and current density within the core will be of interest.

First, the low-frequency (10 kHz) case is considered. Fig. 1(b) illustrates the magnitude of the magnetic flux density at a cross section of the core at a position midway along its length. Referring to the upper portion of Fig. 1(b), the single-layer NiFe, multi-layer NiFe with vacuum interlayer, and multi-layer NiFe with PPY interlayer all have similar, evenly distributed flux density. This illustrates that the typical flux exclusion caused by eddy currents is not occurring in any of these three structures. This is expected as the skin depth of NiFe with the magnetic and conductivity properties detailed above at 10 kHz is approximately 70 μm, which is much thicker than both the single-layer and the multi-layer NiFe structures. It is further observed that there is relatively little flux density in the PPy interlayer (the flux density in the vacuum interlayer was not plotted). This result is expected because it is well-known that the flux density concentrates within higher permeability materials. Fig. 1(c) illustrates the magnitude of the current density within the core at a cross section of the core at a position midway along its length. Referring to the upper portion of Fig. 1(c), there is very little eddy current present in all three core geometries (the magnitude of current density is indicated by both arrow color and size). This is expected as eddy currents should be small at this low frequency. The amount of current is relatively so low compared with that of high frequency that almost nothing is plotted (magnitude of current density is indicated by arrow colors and size). Thus, at low frequency, similar inductance behavior [see Fig. 1(b) and loss behavior [see Fig. 1(c)] would be expected from all three core geometries.

Second, the high-frequency case (8 MHz) is considered. Referring to the lower portion of Fig. 1(b), the single-layer NiFe clearly shows flux exclusion from within the central region of the core, while both the multi-layer NiFe models still show an evenly distributed flux density across the core cross section. Referring to the lower portion of Fig. 1(c), significant eddy current loops are observed in the single-layer core model, while smaller eddy currents are observed in both the multi-layer NiFe models. Thus, at higher frequency, significantly smaller inductance values and higher losses from the single-layer core are expected than from either multilayer core model. Furthermore, little difference in either inductance or loss would be expected between laminations insulated with vacuum or PPy. This modeling result predicts that for these geometries and operating frequencies representative of integrated inductors, PPy interlamination insulation can suppress eddy currents as effectively as perfect (vacuum) insulation,

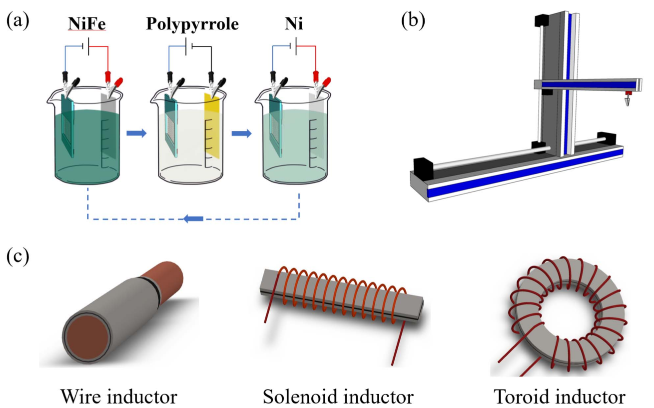

Fig. 2. Schematic drawings of (a) multi-bath electroplating process; (b) automatic electroplating robot; and (c) three different types of inductors tested in this work.

even though PPy has non-zero conductivity and high relative permittivity.

III. Fabrication of Wire, Solenoid, and Toroid Inductors

Experimental validation of the performance of NiFe/PPy cores was carried out through fabrication and characterization of inductor cores with multiple geometries. Magnetic core materials and conductive polymers were sequentially electroplated using a continuous batch process as shown in Fig. 2(a) to create inductor cores. Detailed fabrication procedures including bath compositions, the need for Ni layer, and plating current densities are provided in [17] and [23]. Samples were prepared using a custom-made automated electroplating robot as depicted in Fig. 2(b), where the sample was sequentially immersed into each plating bath and rinsing bath.

Three inductor geometries – a wire geometry, a solenoid geometry, and a toroid geometry as shown schematically in Fig. 2(c) – were fabricated. The wire inductor, in which concentric shells of magnetic and interlayer material are deposited on a wire substrate, is a one-turn inductor where the enamel-coated commercial wire is excited to create magnetic flux. Such wire inductors, using commercial enamel-coated copper wires (diameter 200 μm) sputtered with titanium and gold as substrates for electrodeposition of NiFe and PPy, are a simple model system that does not require lithographic patterning, enabling rapid preliminary testing. The more widely used solenoid and toroid inductor core geometries were also prepared. Both solenoid and toroid inductors were electrodeposited through lithographically patterned photoresist molds, demonstrating the CMOS-compatible potential of this fabrication technology. Electroplated solenoid magnetic cores were rectangles having width and length of 1 and 15 mm, respectively. The disk pattern for toroidal cores had an inner radius of 2 mm and an outer radius of 3 mm.

Each inductor type had three different cross sections of layered structures: thin single-layer NiFe (denoted single-thin NiFe), thick single-layer NiFe (denoted single-thick NiFe), and two thin-NiFe layers sandwiching a middle PPy layer (denoted multi-thin NiFe) as depicted in Fig. 3. The target thickness of the single-thick NiFe was twice that of a single-thin NiFe. The target thickness of each NiFe layer in the multi-thin NiFe was the same as that of a single-thin NiFe. By structuring the test cores in this manner, the single-thick NiFe and multi-thin NiFe have the same total NiFe (i.e., magnetic) thickness, differing only by the presence of the PPy interlayer. For the wire inductor, the targeted thickness of the single-thin NiFe layer was approximately 2 μm, and the targeted PPy thickness (when present) was approximately 200 nm. For the solenoid and toroid inductors, the targeted thicknesses of the single-thin NiFe were approximately 1.5 and 1.2 μm, respectively, while the PPy thickness (when present) was again approximately 200 nm.

To wind the solenoid and toroid inductors, bobbins were fabricated by laser machining commercially available polyimide films of 0.13-mm thickness. The electrodeposited cores were placed in their respective bobbins and wound with 38 American Wire Gauge (AWG) enamel-coated copper wires. Solenoids and toroids were hand-wound to 40 and 36 turns, respectively. The wire ends were then soldered to copper foil pieces to improve electrical connection when interfacing with the characterization tool.

IV. Electrical Characterizations of Wire, Solenoid, and Toroid Inductors

The prepared wire, solenoid, and toroid inductors as shown in Fig. 4(a), (e), and (i) were electrically tested using an *LCR* meter (Hioki IM3536) over the frequency range of 10 kHz–8 MHz. In general, neglecting resonance effects, the presence of eddy currents should manifest as a more rapid increase in resistance (R) with frequency (f), a reduction in measured inductance (L) with frequency, and a reduction in attainable quality factor ($Q = 2\pi f L/R$), compared with inductors of similar geometry and core properties that do not exhibit eddy current losses. To assess the reduction in inductance, the concept of inductance ratio is introduced, in which the measured inductance at a given frequency is divided by its low-frequency (e.g., 10 kHz) inductance value. Thus, an inductance ratio near unity would be expected for inductors with little eddy current loss, while lower inductance ratios would be expected for higher eddy current losses. For the cases of the solenoid and toroid inductors, an air core (i.e., a bobbin winding around a non-magnetic form) was also fabricated for comparison. An air core wire inductor was also measured by determining the self-inductance of a length of wire with no deposited core.

The electrical characteristics of the fabricated inductors will be discussed in the low-frequency and high-frequency regimes, respectively. The low-frequency inductor characteristics at 10 kHz are summarized in Table I. Among the non-air core samples, the single-thin NiFe samples have the lowest inductance values. This is expected, as the single-thin NiFe samples have the thinnest NiFe and thus the smallest total NiFe volume. Meanwhile, single-thick NiFe and multi-thin NiFe samples have similar inductance values as they have comparable total NiFe volumes, also as expected. It is noted that the single-thick NiFe does not have twice the inductance of single-thin NiFe; this is attributed in part to the fact that

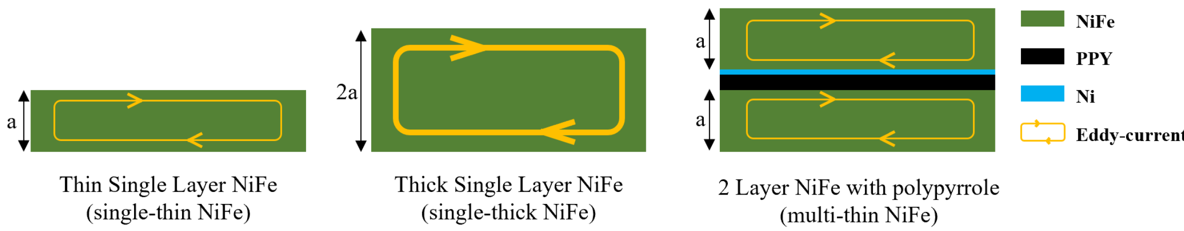

Fig. 3. Cross sections of three different layers fabricated for each type of inductor (wire, solenoid, and toroid inductors) with expected eddy current loops drawn on each magnetic layer.

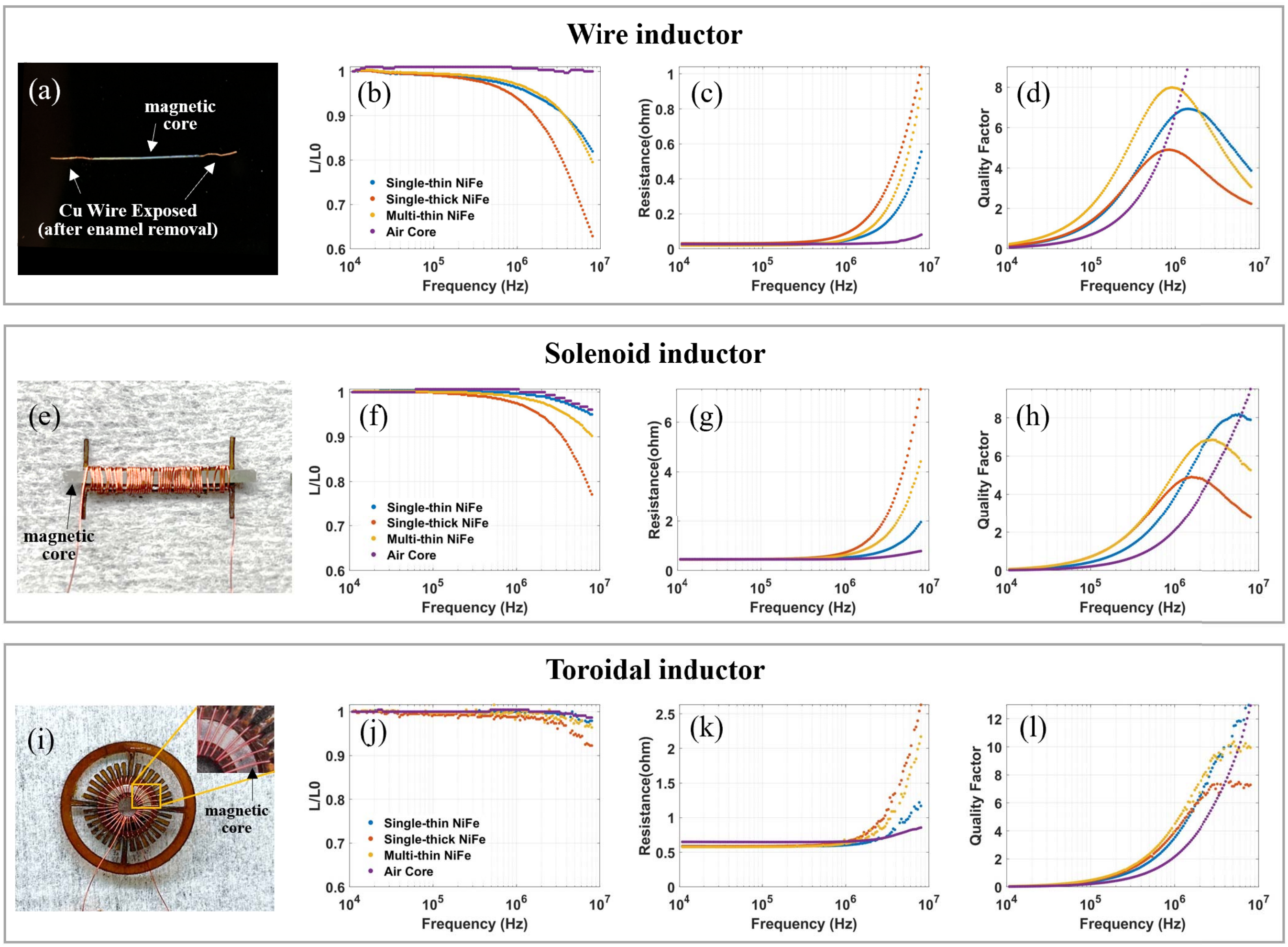

Fig. 4. (a) Sample image, (b) inductance ratio, (c) resistance, and (d) quality factor of a wire inductor. (e) Sample image, (f) inductance ratio, (g) resistance, and (h) quality factor of a solenoid inductor. (i) Sample image; inset: magnified view of bobbin-guided coil winding, (j) inductance ratio, (k) resistance, and (l) quality factor of a toroidal inductor.

the measured inductance includes magnetic flux not only in the magnetic core but also in the air (as well as the expected radial variations in flux in the wire inductor geometry). Note that the air core inductors have non-negligible inductance values as shown in Table I. In addition, as expected, the one-turn wire inductors have the lowest inductance values compared with the multiturn solenoid and toroid inductors.

In the case of resistance, for a given inductor geometry all inductor core types including air core inductors have similar resistances. This is attributed to the fact that at low frequency, the loss contributed by the magnetic core is relatively small, and therefore the resistance is predominantly determined by the winding wire dc resistance values. Since winding wire lengths are similar across all inductor core types for a given inductor geometry, resistances at 10 kHz are similar. Furthermore, referring to Fig. 4, both the inductance and resistance values are relatively stable at low to moderate frequencies since the skin depths over the range are much greater than NiFe thickness.

As frequency increases to several megahertz range, eddy current effects increase, leading to a drop in inductance ratio and increase in resistance as shown in Fig. 4(b), (c), (f), (g), (j), and (k). Inductance ratios expressed as a percentage and resistance values at 8 MHz are summarized in Table II to better quantitatively analyze high-frequency behavior. Inductance drops more in single-thick NiFe than in multi-thin NiFe in

TABLE I
INDUCTANCE AND RESISTANCE AT LOW FREQUENCY SUMMARIZED FOR THE TESTED THREE GEOMETRIES OF INDUCTORS

Geometry	Cross-section	Inductance @ 10 KHz	Resistance @ 10 KHz
Wire Inductor	Single-thin NiFe	52 nH	0.024 ohm
	Single-thick NiFe	73 nH	0.031 ohm
	Multi-thin NiFe	70 nH	0.020 ohm
	Air Core	30 nH	0.027 ohm
Solenoid Inductor	Single-thin NiFe	0.32 μH	0.46 ohm
	Single-thick NiFe	0.53 μH	0.45 ohm
	Multi-thin NiFe	0.51 μH	0.42 ohm
	Air Core	0.15 μH	0.45 ohm
Toroid Inductor	Single-thin NiFe	0.34 μH	0.59 ohm
	Single-thick NiFe	0.41 μH	0.59 ohm
	Multi-thin NiFe	0.45 μH	0.58 ohm
	Air Core	0.22 μH	0.65 ohm

all three inductor geometries even though they have the same total NiFe thicknesses and volumes. For example, in a solenoid inductor, single-thick NiFe retains 77% of its inductance at 10 kHz while multi-thin NiFe retains 90%.

Resistance data show that the resistance of multi-thin NiFe is always lower than that of single-thick NiFe, validating that eddy current loss must be smaller since the total volume of the two is targeted to be the same. Resistance includes not only eddy current loss but also hysteresis loss and miscellaneous loss which are all positively correlated with magnetic core volume.

The quality factor Q of an inductor is the product of angular frequency and inductance divided by resistance ($Q = 2\pi fL/R$). Since the quality factor increases with higher inductance and lower loss, its value for inductors of similar geometry can also be used to assess the efficacy of the PPy interlayer. For air core inductors, since there are no magnetic core losses, Q increases monotonically over the measured frequency range. However, for inductors with magnetic cores, a maximum Q is observed due to increasing core losses with higher frequency. These trends are similar over all three types of inductors. In all cases of wire, solenoid, and toroid inductors, the multi-thin NiFe had a higher quality factor than single-thick NiFe. The frequency at which Q is a maximum is also higher for multi-thin NiFe constructs, showing its suitability in higher operating frequency. Based on these experiments, the effectiveness of PPy in suppressing eddy currents in all three types of inductors, with concomitant increases in operating frequency and reductions in loss, has been demonstrated.

To demonstrate the utility of this technology in thicker cored inductors, as well as demonstrate the fabrication capabilities of this approach, a ten-layer NiFe/PPy solenoid core inductor is fabricated and compared with a single-thick NiFe solenoid core inductor. The electroplated solenoid cores had width and length of 1 and 15 mm, respectively, and were wound

TABLE II
INDUCTANCE RATIOS OF SINGLE-THICK AND MULTI-THIN CORES EXPRESSED AS A PERCENTAGE, RESISTANCE AT HIGH FREQUENCY (8 MHZ), AND MAXIMUM Q-FACTOR (AS WELL AS THE FREQUENCY AT WHICH MAXIMUM Q OCCURRED), SUMMARIZED FOR THE TESTED THREE GEOMETRIES OF INDUCTORS

Geometry	Cross-section	Inductance Ratio @ 8 MHz	Resistance @ 8 MHz	Maximum Q-factor
Wire Inductor	Single-thick NiFe	63%	1.04 ohm	4.91 at 0.8 MHz
	Multi-thin NiFe	80%	0.91 ohm	7.98 at 0.9 MHz
Solenoid Inductor	Single-thick NiFe	77%	7.32 ohm	4.92 at 1.6 MHz
	Multi-thin NiFe	90%	4.41 ohm	6.85 at 2.8 MHz
Toroid Inductor	Single-thick NiFe	92%	2.63 ohm	7.54 at 4.7 MHz
	Multi-thin NiFe	96%	2.17 ohm	10.4 at 5.1 MHz

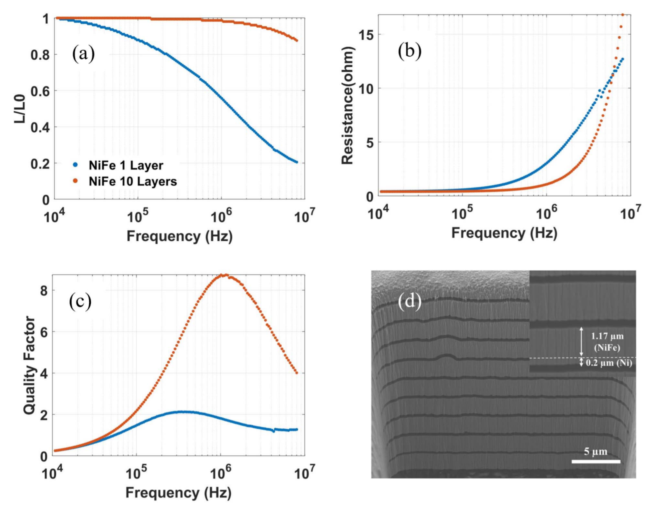

Fig. 5. (a) Inductance ratio, (b) resistance, (c) quality factor, (d) cross-sectional SEM image of the tested single-layer NiFe inductor and ten-layer NiFe inductor. Inset: Magnified image of a ten-layer NiFe inductor to show approximate individual NiFe thickness.

with 40 turns of 38 AWG enamel-coated copper wire. The multilayer core was sectioned using focused ion beam (FIB) and assessed using scanning electron microscopy (SEM). The FIB-SEM image in Fig. 5(d) shows the cross-sectional area where NiFe and Ni appear bright gray, while PPy interlayers appear black. The image demonstrates successful continuous electrodeposition of the thick lamination structure. The inset of Fig. 5(d) shows a magnified view of individual layers in a laminated structure.

We fabricated and compared a single-layer inductor and a ten-layer inductor having similar low-frequency inductance values. We note that in these inductance-matched devices, the measured NiFe thickness of the single-layer inductor (8.9 μm) is thinner than that of the sum of all the individual layers of the multilayer inductor (11.7 μm); however, we further note that the FIB-based thickness measurement is local and may not capture all the thickness variation in all regions of the core. Thus, we have chosen to focus on inductors having similar

TABLE III

INDUCTANCE, RESISTANCE, INDUCTANCE RATIOS EXPRESSED AS A PERCENTAGE, AND MAXIMUM Q-FACTOR (AS WELL AS THE FREQUENCY AT WHICH MAXIMUM Q OCCURRED) SUMMARIZED FOR THE TESTED SINGLE-LAYER NIFE INDUCTORS AND TEN-LAYER NIFE INDUCTORS

	Inductance @ 10 kHz	**Resistance** @ 10 kHz	**Inductance Ratio** @ 8 MHz	**Resistance** @ 8 MHz	**Maximum Q-factor**
Single Layer NiFe	1.57 μH	0.43 ohm	21%	12.7 ohm	2.13 at 0.3 MHz
Multi-layer NiFe (10 Layers)	1.53 μH	0.41 ohm	88%	16.8 ohm	8.74 at 1.2 MHz

low-frequency inductance to show the effectiveness of PPy in suppressing eddy currents at high frequency.

As expected for this thicker multilayer inductor, the eddy current confinement effects are much more prominent in a multilayer inductor as shown in Fig. 5(a)–(c). At high frequency (8 MHz), both the inductance ratio and resistance values show suppression of eddy currents as shown in Table III. The inductance ratio expressed as a percentage is 88% for the ten-layer NiFe core but 21% for the single-thick NiFe core. Both the maximum Q and the frequency at which it occurred were approximately four times higher for the ten-layer NiFe core compared with the single-thick NiFe core. The addition of the relatively thin PPy interlayers boosted inductor performance significantly with little sacrifice in volume. Moreover, we tested ten-layer inductors together with dc bias, as well as using larger ac bias signals. For this tested geometry, the inductors retained 80% of their low excitation inductance up to an IDC of approximately 70 mA and exhibited enhanced inductance over air cores up to approximately 800 mA. With no dc bias, the inductors exhibited little change in inductance up to ac drive signals of 20 mA rms. Such drive current levels have practical application in, e.g., watt-scale conversion of battery voltages for sensor point-of-load switching power conversion, especially at high frequencies. As one example, an application note for an embedded power solution for a CMOS image sensor uses a buck switching converter to step down 2.3–4.8 V (lithium-ion battery) to 1.3 V at 500 mA with an inductor ripple current of 22–37 mA rms [24]. Of course, these measurements should not be taken as indicative of the maximum currents that laminated cores can usefully process; they are geometry- and winding-dependent. By adjusting the number of turns, individual lamination thickness, and a number of layers, inductors having PPy interlayers could function in a wide range of applications.

V. CONCLUSION

We have demonstrated that PPy is a promising material as an interlayer for suppressing eddy current loss in a laminated inductor. High electrical anisotropy of PPy not only enables continuous electrodeposition but also confines eddy currents to each magnetic layer. Finite element analysis showed that PPy is comparable to vacuum up to 8 MHz. Fabrication and characterization of wire, solenoid, and toroid inductors empirically showed PPy does suppress eddy current loss. Inductance was retained and resistance increased less at high frequency compared with a single-layer NiFe sample of the same volume and cross section. From this work, we provided an effective strategy of using an electrically anisotropic material for scalable fabrication of lamination structure and suppression of eddy current loss. Such strategy enables high-frequency operation of an inductor and the use of high B_s material for ultimately miniaturizing power converters.

REFERENCES

[1] H. T. Le, S. Member, Y. Nour, Z. Pavlovic, A. Knott, and F. Jensen, “High-Q three-dimensional microfabricated magnetic-core toroidal inductors for power,” *IEEE Trans. Power Electron.*, vol. 34, no. 1, pp. 74–85, Jun. 2019, doi: 10.1109/TPEL.2018.2847439.

[2] H. Sheng *et al.*, “Recent advances of energy solutions for implantable bioelectronics,” *Adv. Healthc. Mater.*, vol. 10, no. 17, 2021, Art. no. 2100199, doi: 10.1002/adhm.202100199.

[3] M. Yilmaz and P. T. Krein, “Review of integrated charging methods for plug-in electric and hybrid vehicles,” in *Proc. IEEE Int. Conf. Veh. Electron. Saf. (ICVES)*, 2012, pp. 346–351, doi: 10.1109/ICVES.2012.6294276.

[4] C. A. Pardue *et al.*, “Design and characterization of inductors for self-powered IoT edge devices,” *IEEE Trans. Compon., Package., Manuf. Technol.*, vol. 8, no. 7, pp. 1263–1271, Jul. 2018, doi: 10.1109/TCPMT.2018.2803522.

[5] M. Araghchini *et al.*, “Modeling and measured verification of stored energy and loss in MEMS toroidal inductors,” *IEEE Trans. Ind. Appl.*, vol. 50, no. 3, pp. 2029–2038, May 2014, doi: 10.1109/TIA.2013.2291991.

[6] J. Kim, M. Kim, F. Herrault, J. Y. Park, and M. G. Allen, “Electrodeposited nanolaminated CoNiFe cores for ultracompact DC–DC power conversion,” *IEEE Trans. Power Electron.*, vol. 30, no. 9, pp. 5078–5087, Sep. 2015, doi: 10.1109/TPEL.2014.2368140.

[7] J. Kim, J.-K. Kim, M. Kim, F. Herrault, and M. G. Allen, “Microfabrication of toroidal inductors integrated with nanolaminated ferromagnetic metallic cores,” *J. Micromech. Microeng.*, vol. 23, no. 11, Nov. 2013, Art. no. 114006, doi: 10.1088/0960-1317/23/11/114006.

[8] C. O. Mathúna, N. Wang, S. Kulkarni, and S. Roy, “Review of integrated magnetics for power supply on chip (PwrSoC),” *IEEE Trans. Power Electron.*, vol. 27, no. 11, pp. 4799–4816, Nov. 2012, doi: 10.1109/TPEL.2012.2198891.

[9] M. Wang, J. Li, K. D. T. Ngo, and H. Xie, “A surface-mountable microfabricated power inductor in silicon for ultracompact power supplies,” *IEEE Trans. Power Electron.*, vol. 26, no. 5, pp. 1310–1315, May 2011, doi: 10.1109/TPEL.2010.2047406.

[10] J. C. Hertel, Y. Nour, and A. Knott, “Integrated very-high-frequency switch mode power supplies: Design considerations,” *IEEE J. Emerg. Sel. Topics Power Electron.*, vol. 6, no. 2, pp. 526–538, Jun. 2018, doi: 10.1109/JESTPE.2017.2777884.

[11] D. V. Harburg *et al.*, “Microfabricated racetrack inductors with thin-film magnetic cores for on-chip power conversion,” *IEEE J. Emerg. Sel. Topics Power Electron.*, vol. 6, no. 3, pp. 1280–1294, Sep. 2018, doi: 10.1109/JESTPE.2018.2808375.

[12] M. Xu, T. M. Liakopoulos, C. H. Ahn, S. H. Han, and H. J. Kim, "A microfabricated transformer for high-frequency power or signal conversion," *IEEE Trans. Magn.*, vol. 34, no. 4, pp. 1369–1371, Jul. 1998, doi: 10.1109/20.706551.

[13] J. Kim, M. Kim, J.-K. Kim, F. Herrault, and M. G. Allen, "Anisotropic nanolaminated CoNiFe cores integrated into microinductors for high-frequency DC–DC power conversion," *J. Phys. D, Appl. Phys.*, vol. 48, no. 46, Nov. 2015, Art. no. 462001, doi: 10.1088/0022-3727/48/46/462001.

[14] M. Kim and M. G. Allen, "Interlamination insulation design considerations for laminated magnetics operating at high frequencies," *IEEE Trans. Magn.*, vol. 55, no. 8, pp. 1–11, Aug. 2019, doi: 10.1109/TMAG.2019.2910477.

[15] D. Yao, C. G. Levey, R. Tian, and C. R. Sullivan, "Microfabricated V-groove power inductors using multilayer Co-Zr-O thin films for very-high-frequency dc-dc converters," *IEEE Trans. Power Electron.*, vol. 28, no. 9, pp. 4384–4394, Sep. 2013, doi: 10.1109/TPEL.2012.2233760.

[16] J. Kim and M. G. Allen, "Nanolaminated CoNiFe cores with dip-coated fluoroacrylic polymer interlamination insulation: Fabrication, electrical characterization, and performance reliability," in *Proc. Electron. Compon. Technol. Conf. (ECTC)*, 2017, pp. 798–803, doi: 10.1109/ECTC.2017.197.

[17] M. Synodis, J. B. Pyo, M. Kim, H. Oh, X. Wang, and M. G. Allen, "Fully additive fabrication of electrically anisotropic multilayer materials based on sequential electrodeposition," *J. Microelectromech. Syst.*, vol. 29, no. 6, pp. 1510–1517, Dec. 2020, doi: 10.1109/JMEMS.2020.3023347.

[18] B. R. Saunders, R. J. Fleming, and K. S. Murray, "Recent advances in the physical and spectroscopic properties of polypyrrole films, particularly those containing transition-metal complexes as counteranions," *Chem. Mater.*, vol. 7, no. 6, pp. 1082–1094, Jun. 1995, doi: 10.1021/cm00054a007.

[19] G. Sabouraud, S. Sadki, and N. Brodie, "The mechanisms of pyrrole electropolymerization," *Chem. Soc. Rev.*, vol. 29, no. 5, pp. 283–293, 2000, doi: 10.1039/a807124a.

[20] A. C. Cascalheira, S. Aeiyach, P. C. Lacaze, and L. M. Abrantes, "Electrochemical synthesis and redox behaviour of polypyrrole coatings on copper in salicylate aqueous solution," *Electrochim. Acta*, vol. 48, no. 17, pp. 2523–2529, 2003, doi: 10.1016/S0013-4686(03)00295-0.

[21] R. Singh, R. P. Tandon, V. S. Panwar, and S. Chandra, "Low-frequency AC conduction in lightly doped polypyrrole films," *J. Appl. Phys.*, vol. 69, no. 4, pp. 2504–2511, Feb. 1991, doi: 10.1063/1.348688.

[22] J. Feng and D. Thompson, "Permeability of narrow permalloy stripes," *IEEE Trans. Magn.*, vol. MAG-13, no. 5, pp. 1521–1523, Sep. 1977.

[23] M. Synodis, J. B. Pyo, M. Kim, X. Wang, and M. G. Allen, "Lithographically patterned polypyrrole multilayer microstructures via sidewall-controlled electropolymerization," *J. Micromech. Microeng.*, vol. 31, no. 2, Feb. 2021, Art. no. 025008, doi: 10.1088/1361-6439/abd098.

[24] *TPS6267x 500-mA/650-mA, 6-MHz High-Efficiency Step-Down Converter in Low Profile Chip Scale Packaging (Height <0.4mm)*, document TPS62674 Datasheet, Texas Instruments, Dallas, TX, USA, Apr. 2010.

Jun Beom Pyo (Graduate Student Member, IEEE) received the B.S.E. and M.S.E. degrees in materials science and engineering from the University of Pennsylvania, Philadelphia, PA, USA, both in 2012, where he is currently pursuing the Ph.D. degree with the Electrical and Systems Engineering Department.

From 2013 to 2017, he was a Research Scientist with the Korea Institute of Science and Technology (KIST), Seoul, South Korea. His current research interests include designing and miniaturizing inductors for switching power converters.

Xuan Wang received the B.Eng. degree in electrical engineering and automation from Fudan University, Shanghai, China, in 2018, the B.Eng. degree in electronic and electrical engineering from the University of Birmingham, Birmingham, U.K., in 2018, and the M.S. degree in nanotechnology from the University of Pennsylvania, Philadelphia, PA, USA, in 2020, where she is currently pursuing the Ph.D. degree in electrical and system engineering.

Her research interests include integrated magnetics and microfabrication.

Minsoo Kim (Member, IEEE) received the B.S. and M.S. degrees in electrical and computer engineering from Seoul National University, Seoul, South Korea, in 2006 and 2008, respectively, and the Ph.D. degree from the Georgia Institute of Technology, Atlanta, GA, USA, in 2016.

He is currently a Hardware Engineer with Apple Inc., Cupertino, CA, USA. His graduate research involved MEMS-enabled, laminated magnetics toward scalable power inductor technology with improved energy/power densities.

Hanju Oh (Member, IEEE) received the B.S. degree in electrical and computer engineering from Hanyang University, Seoul, South Korea, in 2010, and the M.S. and Ph.D. degrees in electrical and computer engineering from the Georgia Institute of Technology (Georgia Tech), Atlanta, GA, USA, in 2014 and 2017, respectively.

He was a Post-Doctoral Fellow with the Electrical and Systems Engineering Department, University of Pennsylvania, Philadelphia, PA, USA. He is currently with Apple, Inc., Cupertino, CA, USA. His current research interests include 3-D electronic system integration, flexible microsystems, biomedical sensors and actuators, and nanofabrication technology.

Dr. Oh received the Best Oral Session Paper Award at the IEEE Electronic Components and Technology Conference (ECTC) in 2016, the Charles Hutchins Educational Grant Award from the Surface Mount Technology Association (SMTA) and the Circuits Assembly Magazine in 2015, the best student paper awards at the IEEE Global Interposer Technology (GIT) Workshop in 2014, and the Best Poster Award in the thermal track at the Intersociety Conference on Thermal and Thermomechanical Phenomena in Electronic Systems (ITherm) in 2014.

Robert Kauffman received the bachelor's degree in physics from the Juniata College, Huntingdon, PA, USA, in 2020. He is currently pursuing the master's degree in nanotechnology with the University of Pennsylvania, Philadelphia, PA, USA.

He is currently searching for a career in the semiconductor industry after graduation in May 2022. His interests include process engineering, lithography, and microelectromechanical systems.

Mark G. Allen (Fellow, IEEE) received the B.A. degree in chemistry, the B.S.E. degree in chemical engineering, and the B.S.E. degree in electrical engineering from the University of Pennsylvania, Philadelphia, PA, USA, all in 1984, and the S.M. degree in chemical engineering and the Ph.D. degree in microelectronics from the Massachusetts Institute of Technology, Cambridge, MA, USA, in 1986 and 1989, respectively.

In 1989, he joined the faculty of the School of Electrical and Computer Engineering, Georgia Institute of Technology, Atlanta, GA, USA, ultimately holding the rank of Regents' Professor and the J. M. Pettit Professorship in Microelectronics, as well as a joint appointment with the School of Chemical and Biomolecular Engineering. In 2013, he became the Alfred Fitler Moore Professor of electrical and systems engineering and the Scientific Director of the Singh Nanotechnology Center, University of Pennsylvania. His research interests include development and application of new micro- and nano-fabrication technologies, as well as MEMS.

Dr. Allen received the IEEE 2016 Daniel P. Noble Award for contributions to research and development, clinical translation, and commercialization of biomedical microsystems. He was the Co-Chair of the IEEE/ASME MEMS Conference and the Chair of the 2016 Solid State Sensors, Actuators, and Microsystems Conference. He is a Co-Founder of multiple MEMS companies, including Enachip, Rocky Hill, NJ, USA. He was the Editor-in-Chief of the *Journal of Micromechanics and Microengineering*.